Technische Universität München
Lehrstuhl für Aerodynamik und Strömungsmechanik

Studying the Effects of Shock-Boundary Layer Interaction by Means of Implicit Large Eddy Simulation

Oana Petrache

Doctor of Philosophy Thesis

Supervisor:	Univ.-Prof. Dr.-Ing. S. Hickel
Supervisor:	Univ.-Prof. Dr.-Ing. N.A Adams

The thesis was done at the Technische Universität München, Fakultät für Maschinenwesen, as part of the Graduiertenkolleg 2/1095 programme, funded by German Research Foundation.

Oana Petrache
opetrache@yahoo.com

Released 01.11.2019
Typesetting LaTeX

PREFACE

I decided to write the preface because all stories start with “Once upon a time“, all stories need a frame. This is mine.

Thanks to my dad, who always showed me constellations on the clear unaltered sky of Drăgăşani, I wanted to become an astronomer. Because I couldn't do that in Romania, I was somehow forced to look other way. My 17-years old reasoning went like ” *What is closer to the sky?*” . The answer was right there in front of me, defying gravity: airplanes. They were my second fascination after Orion, Cassiopeia, Scorpio, the Pleiades and so on. So I took on the challenge. It was this challenge that brought me to Munich, it was because of this challenge I ended up doing my PhD thesis as part of a group who works on scramjets. The word scramjet, was barely uttered during my studies, not because people didn't know what it was, but because no one even dared to believe in their existence, no one dared to think that somewhere in this world there are people dreamy enough to invest their lifetime work in such a sci-fi topic.

This is why I became an engineer. Not because I wanted to find new solutions, to solve new puzzles, but because I simply wanted to find out *how it's made.* I wanted to respond to my incontrollable need to know more.

In this frenzy there are lot of people I left behind or discovered. All of them have supported and bared with me and deserve mentioning here. I would not have been here, hadn't it been for the support and constant encouragement of my parents. So, mama şi tata, vă mulţumesc!

Thanks also go to my professor, Nikolaus Adams, who, as busy as he was, always found time for our Tuesday meeting and useful scientific advice given in amusing ways. This was dubbed by a rich input, vision and help from Stefan, a dedicated geek and friend. Thank you both for making this possible!

In the frames of the GRK 1095 project, my fellow colleagues made my PhD time a little less serious and a little more relaxed and funny. So, Anne-Marie, Arianna, Hannes, Christian, Oli, Vladimir, Jiby, Marc, etc, thank you guys for the nice summer schools and the Black Forrest meetings!

Also thanks to the colorful LFA Institute. Patrick, Dominic, Stefan, Sebastian, Toni, Flo, Tobi, Andi and the others, you know that my life at TUM would not have been the same, had it not been for your laughter and good spirit.

CONTENTS

LIST OF FIGURES

LIST OF TABLES

NOMENCLATURE

Roman Symbols

Ma	Mach number
Pr	Prandtl number
Re	Reynolds number
St	Strouhal number
a	integration bound
$a_1 - a_5$	structure parameters of the flow
a_{ij}	Reynolds stress anisotropy tensor
$\overline{b}$	average separation bubble length
c	speed of sound
C	constant in the law of the wall
C_f	friction coeffieicient
C_p	specific heat at constant pressure
C_V	specific heat at constant volume
d	entropy spot diameter
e_{kin}	kinetic energy
E	total energy
f_{ES}	entropy spot frequency
f_S	characteristic frequency
$g(r, s)$	function characterizing the intensity of the separation region (see Ref. Piponnau *et al.* [31])
H_{12}	shape factor based on displacement and momentum thicknesses
k	von Kármán constant
k	thermal conductivity
L	integral length scale
L_{ref}	reference length
L_{sep}	separation length
N	number of points
p	static pressure

q	heat flux
r	entropy spot radius
$\overline{R^z_{\alpha\alpha}}$	autocorrelation function in spanwise direction
t	time
T	static temperature
u_τ	wall friction velocity
$u \equiv U$	streamwise velocity component
$v \equiv V$	wall-normal velocity component
$w \equiv W$	spanwise velocity component
$\overline{u}_{VD}$	Van Driest transformed velocity
u^+_{log}	logarithmic law of the velocity based on y^+
$\overline{x}_s$	average separation point
$\overline{x}_r$	average reattachment point
$\|_a - \|\|_b$	invariant map of Reynolds stress anisotropy tensor
$\overline{\rho' u'}$	streamwise component of turbulent mass flux
$\overline{\rho' v'}$	wall-normal component of turbulent mass flux
$\overline{\rho' w'}$	spanwise component of turbulent mass flux
$\overline{u' u'}$	streamwise component of the Reynolds stress tensor
$\overline{v' v'}$	wall-normal component of the Reynolds stress tensor
$\overline{w' w'}$	spanwise component of the Reynolds stress tensor
x^+	streamwise velocity component in viscous units
y^+	wall-normal velocity component in viscous units
z^+	spanwise velocity component in viscous units

Greek Symbols

α	stretching parameter
β	angle of the shockwave with the freestream
δ	boundary layer thickness
δ^*	displacement thickness
δ_{ij}	Kronecker delta
θ	momentum thickness
θ	angle of the boundary layer structures
ϵ	entropy spot amplitude

λ	length of a boundary layer superstructure; the size of the largest eddies
λ_2	visualization quantity for turbulence
μ	kinematic viscosity
$\Phi(Mc)$	function that qualifies the effects of compressibility (see Ref. Piponnau *et al.* [31])
Φ	recycled quantity
Φ	equivalence ratio
$\xi = \frac{x-x_r}{x_r-x_s}$	non-dimensional streamwise coordinate
ρ	density
τ_w	wall shear stress
ζ	angle of the boundary layer structures
ω	vorticity

Other Symbols

$\bar{\cdot}$	mean value (Reynolds filter)
$\cdot'$	fluctuation

Subscripts

0	reference state
∞	free-stream property
av	average
$crit$	critical
f	final
inc	incompressible
inf	inflow plane
int	interaction
r	recycling plane
$recy$	recycling plane
ref	reference value
KS	Kármán-Schoenherr
BL	boundary layer

POW	power law
sep	separation
$Suth$	Sutherland
t	total
t	turbulent
x	in streamwise direction
y	in wall-normal direction
z	in spanwise direction
w	property at the wall
δ	based on δ
θ	based on θ
τ	based on wall friction

Acronyms

1-D	one-dimensional
2-D	two-dimensional
3-D	three-dimensional
ALDM	adaptive local deconvolution method
AST	average starting time
CTBL	compressible turbulent boundary layer
CTBLC	LES coarse simulation of compressible turbulent boundary layer
CTBLM	LES medium simulation of compressible turbulent boundary layer
CTBLF	LES fine simulation of compressible turbulent boundary layer
DF	digital filter
DNS	direct numerical simulation
ES	entropy spot
FTT	flow-through time
GSRA	Guarini strong Reynolds analogy
HSRA	Huang strong Reynolds analogy
LEO	low Earth orbit
LES	large eddy simulation
LIA	linear interaction analysis
LSM	large scale motion

NIP	nominal impingement point
NRP	nominal reattachment point
ODE	ordinary differential equation
PIV	particle image velocimetry
RANS	Reynolds-averaged Navier-Stokes
RRT	rescale-recycle technique
SEI	schockwave-entropy spot interaction
SR	sampling rate
SRA	string Reynolds analogy
SWBLI	shockwave-boundary layer interaction
SWLBLI	shockwave-laminar boundary layer interaction
SWTBLI	shockwave-turbulent boundary layer interaction
TS	time step
WENO	weighted essentially non-oscillatiory

— CHAPTER ONE —

INTRODUCTION

1.1 Motivation

Ever since 1903, when the Wright brothers have achieved the first sustained controlled heavier-than-air manned flight, the desire for flying higher and faster has never seized for mankind. It is because of this desire we nowadays have a variety of aircraft propulsion systems available. The wide utilisation os the gas turbine ranges from commercial airline carriers to $Ma = 2+$ fifth generation jet fighters. In this case, the air captured by the inlet, the so-called working fluid, passes firstly through the compressor in order to achieve high enough static pressure necessary for an efficient combustion process. The fluid is then injected with fuel, combustion takes place and the resulting composition is expanded through the turbine in the nozzle. As pointed out in the diagram of specific impulse over Mach number (see Fig. 1.1), the efficiency of such aero-propulsive systems decreases dramatically with increasing incoming flow velocity, the upper speed limit being at $Ma = 3$. This limit is overcome with another type of airbreathing engine configuration, namely ramjet. In the range $Ma = 3 \div 6$ we deal with a subsonic combustion (ramjet), while for speeds exceeding $Ma = 5$, the supersonic combustion ramjets, or scramjets, give less pressure losses due to compression, and hence, higher combustion efficiency. Given its airbreathing nature, the ramjet technology seems to be a good candidate for replacing the space shuttle or any other vehicle needing exclusively rocket propulsion for accessing the Earth Orbit. In rocket engines, the fuel is embedded in the vehicle, but one has to also carry huge oxidiser reservoirs. In the case of the space shuttle they were then dumped in the Low Earth Orbit (LEO), subjecting satellites or other objects orbiting the Earth to the Kessler effect.

The ramjet technology is almost as old as the first manned flying machines. In 1913, René Lorin was granted a patent for a device resembling a scramjet. Unfortunately, little could be done at the time due to lack of materials able to sustain such high heat loads. As time passed by, several attempts were made in that matter, names as Albert Fono (1915), Fritz Zwicky (1940), Eugen Sänger (1941), René Leduc (1949) having brought their contribution to ramjet development. In 1949 one of the first manned ramjet-based vehicle, Leduc 0.10, flew.

The scramjet file for patent goes back to Frederick S. Billig in 1964, but it was only received by beginning of the 1980s due to an order of secrecy protecting the knowledge

issued by the American government. A notable contribution to scramjet research was brought in the late 1980s beginning of 1990s by the National Aerospace Plane (NASP) program. The aim was to build two vehicles capable of single-stage-to-orbit (SSTO), as well as vertical take off and landing from common runways. At the same time, a concept of Eugene Sänger was relaunched in Germany. Sänger II was designed as a reusable vehicle composed from a superposition of two bodies: a combined turbojet/ramjet-SCRAMjet cycle aircraft and a rocket-engine aircraft. Scramjet development was to know a second hype in the years 2000. HyShot (Australia) or Hyper-X (USA) are just a few of the successful attempts to test supersonic combustion engines during the past decade. Nowadays, scramjet research programs exist all over the world: USA, Australia, Germany, France, UK, Russia, Japan to name just a few.

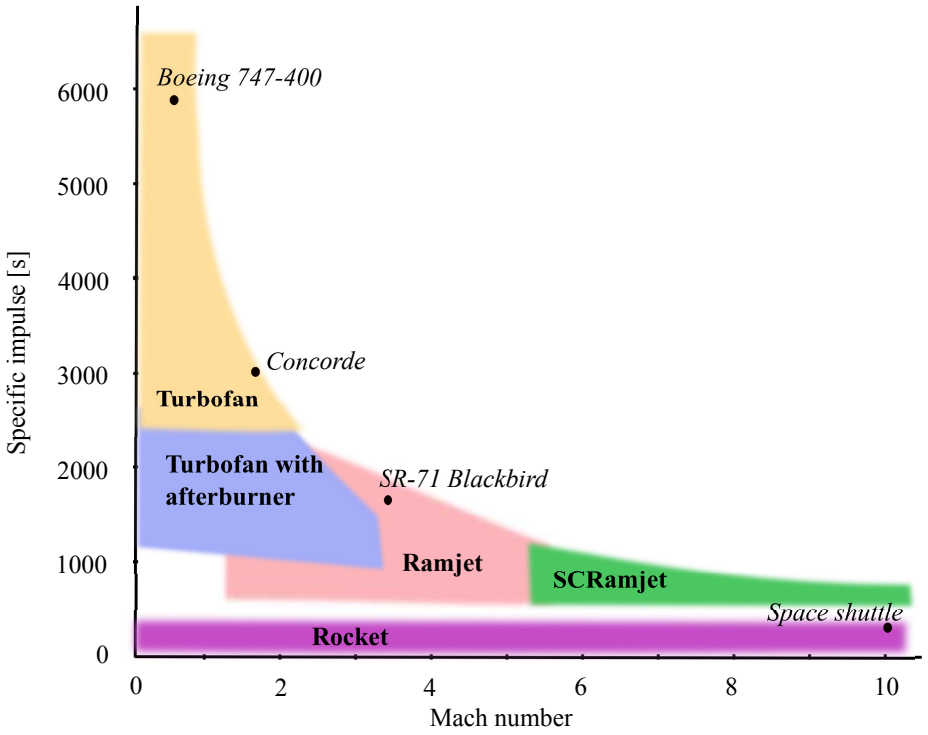

Figure 1.1: Specific impulse over Mach number

There are several reasons for the interest in the scramjet technology. One of them is its structural simplicity. Having to operate at hypersonic speeds, the omnipresent compressor from standard turbojet or turbofan engines is replaced by an appropriate combination of ramps meant to compress the incoming air through a shockwave system. This significantly reduces the weight of the entire engine, not to mention it eliminates probable failure sources due to fatigue.

Another reason for scramjet's appeal falls among finances. Reusable scramjet-based

aircrafts can fly fast, making it possible to unite any two points on the surface of the Earth in around three hours, considering an average velocity corresponding to $Ma = 7$. This would bring the air transportation industry to a totally new level. On the other hand, there is the significant contribution such a scramjet vehicle would have to space transportation. Before Antlantis' last flight in July 2011, every trip the space shuttle made to the orbit resulted in huge costs for the fuel, oxidiser and tanks of the solid rocket boosters needed for the shuttle to reach the Earth escape speed. Some sort of combined scramjet/rocket engine would be able to bring payloads to International Space Station or perform any kind of servicing mission with less financial effort.

The American poet and essayist Ralph Waldo Emerson explains the term "compensation" as "For everything you have missed, you have gained something else; and for everything you gain, you lose something else". As far away as the scramjet lies from the field of Mr. Emerson, the saying very much applies here as well. The advantages of such a propulsion system come to face some key problems.
Firstly, it cannot operate at low velocities, meaning an aircraft equipped only with a scramjet could not take off by itself from a conventional runway. The way out is to add an extra cycle, such as a turbofan. This would increase the complexity and weight of the vehicle. Another possible problem is that material development does not keep up with the technology. The supersonic combustion takes place at stagnation temperatures on the order of $3500K$, posing a challenge for materials in use.
And even having surmounted the above mentioned impediments, a great challenge still lies ahead. The design of a scramjet engine is an extremely intricate work. Roughly speaking, the flow inside it is characterised by a series of shocks generated by geometry change; these shocks impinge on turbulent boundary layers and generate separation of the near-wall flow; the isolator has the distinctive role of hosting the shock train, which is the way the flow is adjusting to the high pressure produced by the fuel combusted downstream; as the name says, the combustion chamber is the place where fuel is freed in the compressed airstream through wall ports or strut injectors, mixed and burned; through the nozzle, the flow is expanded and accelerated in order to produce thrust. For simplification purposes, in an initial research phase, one can consider a 2-D flow path, owing it to rectangular inlet and combustor cross-sections. This is of course true up to the point when we consider the vehicle is performing a turn manoeuvre by changing its yaw angle (Hohn and Gülhan [23]) or if we acknowledge the presence of interacting shocks or concurrent boundary layers. In all these cases, the flow path from inlet to nozzle is completely different than the 2-D case.
The engine performance is also affected. If we add to this the high thermal loads, which the combustion chamber and nozzle have to withstand, another problem rises, namely

cooling. Passive or active, cooling is a way to influence wall temperature and hence, near-wall flow behaviour.
The injector type and geometry have another important say in the overall flow path. Wall injectors are known not to have enough penetration in the freestream and therefore affecting more the flow close the the wall, while strut injectors adress the combustion chamber core flow, where shocks traverse the fuel shear layer, amplifying turbulent mixing and combustion (see Sachs and Wagner [39]). In addition to the internal flow, we also have to be aware of the large sensitivity of the structure to the aerothermodynamics forces. Having said that, it is quite clear that scramjet development one needs a systematic approach.

1.2 Contribution of This Work

In 2005, the German Research Training Group (GRK 1095) was initiated on the base of already existing scientific know-how in the field of scramjet technology and hypersonic vehicles design. The main goal of this project is the aero-thermodynamic design of a scramjet propulsion system which integrates all parts of such an engine, i.e. forebody, inlet, isolator, combustor and nozzle, and where each part is optimised for the chosen engine design point. Furthermore, thermo-mechanical analyses with regard to high-temperature materials for the combustion chamber, as well as numerical system analyses of the complete engine are carried out. Even though an actual in-flight experiment is not part of the Research Training Group, the described scramjet demonstrator represents the overall objective of all projects involved. In that light, each project from GRK 1095 develops individual goals, which are linked to the other projects.
The present investigation was carried out as subproject of the GRK 1095. Its focus is on turbulent mixing induced by shock-turbulent boundary layer interaction (SWTBLI) in the presence or absence of heat sources. As pointed out, the flow in a supersonic combustion engine is shock dominated and is characterised by a residence time of the order of milliseconds. In this short interval, fuel has to be injected, mixed and burned before it exits through the nozzle. Among others, a good fuel/air mixing is one of the factors, which greatly contribute to an efficient combustion.
The classical ways of influencing the mixing is through the injector choice. The impending choices are wall injectors: perpendicular, parallel (see Fig. 1.2) or inclined with respect to the freestream direction, they rely on diffusion-based mixing. The immediate advantage of such a fuel injection procedure is its simplicity in terms of construction: situated in the combustion chamber walls, the injector's body is not exposed to high temperatures, therefore a cooling strategy is not needed. Also, in case of having hydro-

gen fuel, due to its low storage temperatures (around $20 - 30K$), the injection from a backward facing step provides film cooling for the combustor walls, as well as reduced freestream pressure losses. In all three injection cases (parallel, perpendicular or angled), there is only one diffusion boundary. This affects the combustor length, which has to be large enough to allow for an efficient mixing, adding weight to the entire engine. The one diffusion boundary problem may also cause quenching of fuel next to the cold wall (Sachs and Wagner [39]), implying a low penetration of fuel in the freestream and therefore a poor mixing and combustion efficiency.

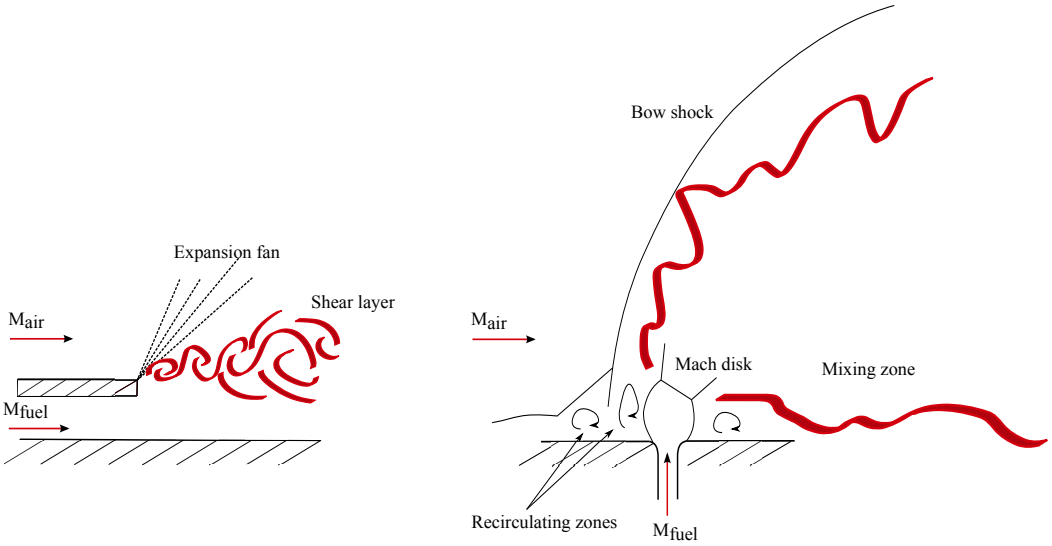

Figure 1.2: Examples of wall injectors

Changing perspective, we find the penetrative injectors, the ones that disturb the flow field. Hypermixers are injectors that due to a pressure difference between lower and upper part of the geometry, introduce streamwise vortices in the flow field (see Fig.1.3). These vortical structures increase turbulent fluctuations perpendicular to combustor flow direction, at the expense of fluctuations parallel to flow direction. The increased spanwise turbulent fluctuations can break down large 2-D structures into smaller turbulent vortices essential for mixing and diffusion. Hypermixers can be found as swept/unswept ramps mounted on the wall or as in-stream alternating wedges. For wall-mounted hypermixers the positive effect to fuel/air mixing is counterbalanced by insufficient penetration in the freestream. In the case of a strut type of hypermixer, the fuel is injected into the center of the combustor airflow, with an even distribution along the injector's length. Also, a subsonic wake region allows for combustion flame holding. There is, however, a negative aspect to the strut-type injectors: their presence in the freestream is followed by shocks and consequently total pressure losses, as well as increased drag.

As we have seen, from the injector side, there is no win-win situation. For maximising the fuel/air mixing, in GRK 1095 we combined the advantages of a lobbed strut injector with two wall injectors located downstream of the first one.

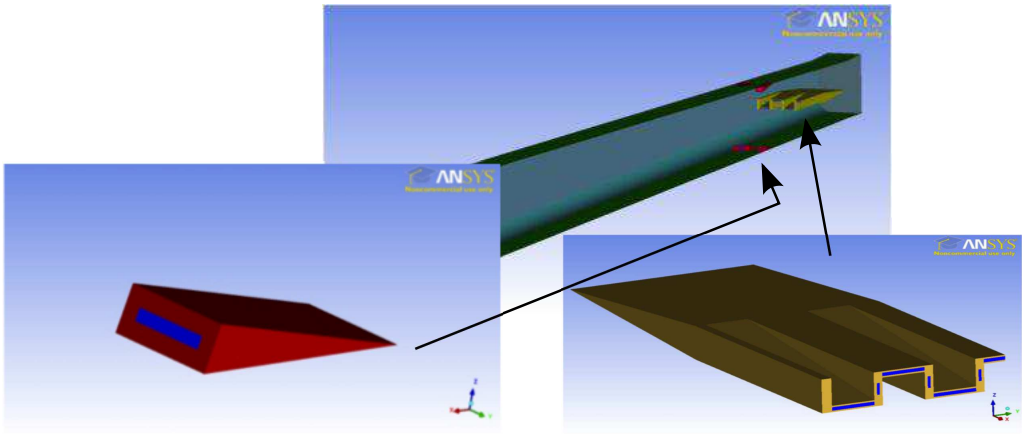

Figure 1.3: Hypermixers

The topic of the present work is numerical simulations of SWTBLI. Another isde of this near-wall flow phenomenon is its consequential contribution to turbulent mixing. Roughly speaking, SWTBLI results in boundary layer separation, oscillation of the reflected shock and turbulence amplification behind the boundary layer reattachment point (Pirozzoli and Grasso [32], Pirozzoli *et al.* [33], Beresh *et al.* [3], Bookey *et al.* [4], Priebe *et al.* [35], Wu and Martin [42], Shahab [40]). Another source of vorticity production is the interaction of an entropy wave with a shock (Hussaini and Erlebacher [25]).
In the context of the GRK 1095 scramjet combustor, which contains a strut injector and two wall ports located downstream of the chamber, oblique shocks are generated by the presence of the strut in the main flow field. The entropy source might be represented by hotter or colder regions (with respect to the freestream temperature) generated by the combustion process and located downstream of the strut, but upstream of the wall injectors. These hot or cold fluid "patches" are then convected through oblique shocks. The result in terms of turbulence amplification is a superposition of the effects of shock-turbulent boundary layer and shock-entropy spot interactions. This turbulence enhancement should have a positive effect on the fuel/air mixing needed downstream, by the following wall injectors.

1.3 Outlook

This work will be structures as follows: in the next chapter (Chapter 2) we set the frames around our study by presenting a bit of background in the matter of shockwave-boundary layer interaction. After that, (Chapter 3) we introduce the numerical tools used in our investigation. In Chapter 4 we prove that the chosen numerical method is suited for our endeavour, by using it in a wall-bounded flow simulation. The last two Chapters 5 and 6 are dedicated to the study of shockwave-turbulent boundary layer interaction with and without entropy disturbances.

— CHAPTER TWO —

FLOW PHYSICS

2.1 Shockwave-Boundary Layer Interaction

Depending on the Reynolds number, $Re_x = \rho_\infty U_\infty L_{ref}/\mu_\infty$, based on local freestream quantities (ρ_∞, U_∞ and μ_∞) and the flat plate length (L_{ref}), a boundary layer can be laminar or turbulent. The interaction topology has, in both cases, some common features: when faced with a high enough adverse pressure gradient imposed by the incident shock, the boundary layer separates and a subsonic reverse flow region builds up underneath it. The so-called "reflected shockwave" is actually a series of compression waves caused by the separation bubble and the outward displacement of the streamlines. The actual incident shockwave is reflected as an expansion fan. The boundary layer reattachment causes another series of weaker compression waves (see Fig. 2.1).

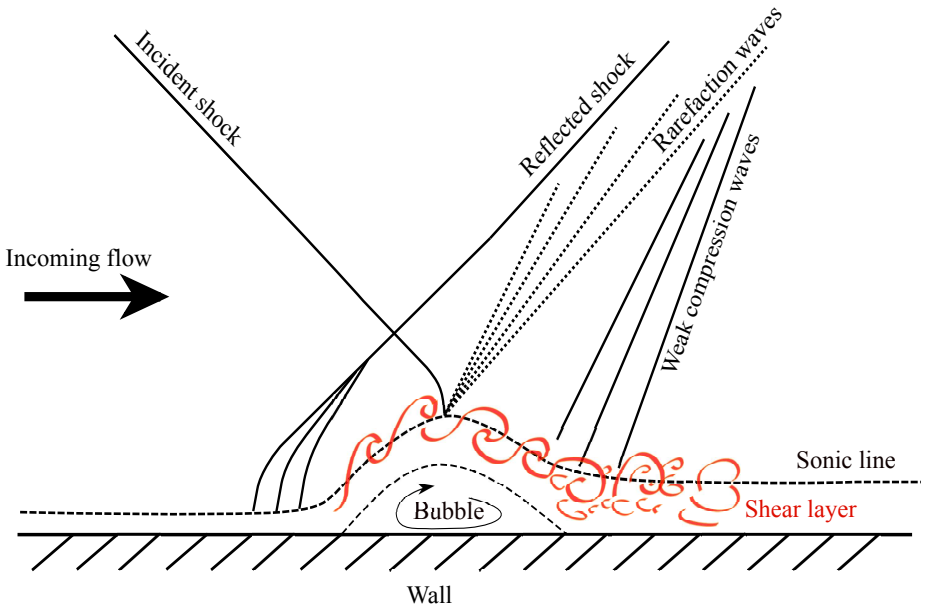

Figure 2.1: Shockwave-turbulent boundary layer interaction

From subsonic transporters to hypersonic air-breathers, each of these aircrafts face, locally or globally, supersonic flows, which often produce shock-induced boundary layer

separation. Given the large scale of industrial applications, it is reasonable to assume one is dealing with turbulent boundary layers. In this case, shockwave-boundary layer interaction (SWBLI) becomes an instationary phenomenon and is characterised by low-frequency reflected shock motions and a significant change in local flow topology. The shock movement can be recognised in wall pressure signals and has specific frequencies of two orders of magnitude lower than the characteristic energetic scales of the incoming turbulent boundary layer. Even if the shock motion relative to the system is unimportant, it causes high local aerodynamic and thermal stresses, which globally affect the system. Being such a determinative constraint in aircraft construction, SWBLI has received considerable attention over the past 70 years. A consistent inventory of the first investigations concerning this flow behaviour can be found at Adamson and Messiter (Adamson and Messiter [1]).
In the present study we will only refer to shockwave-flat plate boundary layer interactions, a configuration frequently found in a supersonic combustion chamber of a scramjet.

2.1.1 Shockwave-Laminar Boundary Layer Interaction

For laminar flows, a rather weak pressure rise is enough for separating the wall bounded flow. The separation point moves further upstream with increasing the shock strength, p_3/p_1, where p_1 is the freestream pressure before the incident shock and p_3 is the freestream pressure after the reflected shock) The incident shock's penetration in the boundary layer is proportional to its strength, hence the higher the shock strength, the closer to the wall the incident shock gets. The pressure distribution characterising a shockwave-laminar boundary layer interaction (SWLBLI) exhibits a plateau between p_1 and p_3. The separation bubble is symmetric and triangular, but it has an unsymmetrical convergence of the streamlines. Moreover, it was observed (Katzer [27]) that depending on the shock strength, a secondary recirculation bubble can develop within the first one, giving rise to a secondary negative peak in the wall shear stress, before the reattachment point.
Before computational power was at hand, researchers used approximate methods based on simplifications and presumptions in order to estimate the flow behavior in a SWLBLI. One of the most popular ones is the *triple-deck theory*: the boundary layer is divided in three "decks", each of them being scaled differently and having different dominating processes. The "upper deck" has a thickness on the order of $\mathcal{O}(Re^{-3/8})$ and is dominated by an irrotational flow; the "main deck", $\mathcal{O}(Re^{-1/2})$, contains most of the boundary layer and its upward displacement under the influence of the impinging shock; the "lower deck" is a very thin layer, $\mathcal{O}(Re^{-5/8})$, close to the wall, where viscous effects

are dominant. All three layers are governed by different equations, corresponding to the simplifications made, and boundary conditions set according to the neighbouring layer. A comprehensive study on the applicability of this theory on a compression corner can be found at Rizzetta *et al.* [37].
Indeed some years later, Katzer [27] found the same limitations of the triple-deck theory as Rizzetta: although pressure scalings in the free interaction zone ("the free interaction zone" was firstly defined by Chapman *et al.* [5] as a region in the vicinity of separation where flow properties do not depend on downstream phenomena) seem to match, the length of the separated region is overestimated by $2-3$ times. More than that, Katzer found two mechanisms characterising the laminar shock reflection: a *global* one, having as a length scale the separation bubble, which depends only on the shock strength and Reynolds number, with powers of 3 and 1/2, respectively, and a *local* one governed by the shear stress at the beginning of the interaction and boundary layer edge Mach number.

Nowadays, however, there is no need for exhaustive derivation of simpler equations to describe a laminar boundary layer separation. We have the computer resources to run such simulations in no time. Plus, the triple deck theory, as well as other integral methods (see Lees and Reeves [29]), proved that the general characterisation of flow length scales and geometry has certain constrains, which, when overstepped, lead to inaccurate predictions.

Although the unstable reflected shock behavior is, as we will see later, mostly linked to the turbulent character of the incoming boundary layer, recent studies (Robinet [38]) trace it back to bifurcations in SWLBLI. In his DNS, he varied the shock strength, as well as the spanwise domain size, following that beyond a given incident shock angle, $\theta > 32.7°$, and a certain span, $L_z = 0.8 l_{bubble}$ (where l_{bubble} is the separation bubble length), deviations in Z-direction from the initially 2-D the flow field are observed within the reverse flow region (in a mathematical sense, the phenomenon of change in the topology of a given family of ODEs and their solution is known as a "bifurcation"). A low frequency of $\approx 700Hz$ characterises the unsteady separated flow. Whether or not this is the precursor for reflected shock unsteadiness in shockwave-turbulent boundary layer interaction needs further investigation.

2.1.2 Shockwave-Turbulent Boundary Layer Interaction

In the case of a shockwave-turbulent boundary layer interaction (SWTBLI) the flow topology is similar to a laminar shock reflection. There are, however, some important

differences: a turbulent boundary layer needs a higher pressure rise in order to separate and the detachment point travels slower upstream with increasing the shock strength; the interaction zone is highly three-dimensional – in Fig. 18 from the paper of Pirozzoli and Grasso [32], we notice the scatter of the reverse flow region depicted through negative values of the skin friction coefficient; the reflected shock foot exhibits wrinkles generated by the turbulent structures in the boundary layer; due to the streamwise velocity sign change over the interaction, a shear layer forms on top of the recirculation bubble and persists till further downstream, locally amplifying turbulence. Probably the most argued property of SWTBLI is the reflected shock low-frequency oscillation. The reason for this behaviour has been intensively disputed in the research community over the last few decades.

Shockwave dynamics tells us that shocks can be displaced under upstream or downstream (when a subsonic separated flow region is involved) influences. Depending on the downstream conditions, they can be frequency selective or not, damping an excitation, be neutral to it or act like a low-pass filter and amplify lower frequencies of that disturbance. Relying on this frequency selective property, Plotkin [34] hypothesised that the reflected shock oscillation is determined by the *incoming turbulent boundary layer fluctuations*. Namely, from the broad turbulent frequency spectrum contained in the wall bounded flow, the shock would be responsive to the lowest frequencies while damping higher frequencies. This mechanism would induce a displacement of the shock foot, which would eventually be linearly restored. Based on these assumptions, Plotkin was able to successfully match experimental pressure spectra. Although his postulation correctly implied that there is a connection between incoming turbulence and its passage through the shockwave, it didn't, however, give a general information on the time scales involved in the process. This conclusion motivated a several further studies about the effect of the upstream boundary layer physiology on the interaction.

Based on PIV measurements Ganapathisubramani *et al.* [11] concluded that the large-amplitude low-frequency behaviour of the reflected shockwave follows the passage of boundary layer *long coherent superstructures* through its foot. The excited frequency in this case would be $U_\infty/2\lambda$, where U_∞ is the freestream velocity before the interaction and λ is the length of the superstructure.
Humble *et al.* [24] reinforced that claim by performing a three-dimensional tomography of the interaction structure. In their model, the boundary layer is composed from an intercalation of elongated high, respectively low, velocity structures interfaced with wall-normal vorticity regions. Convecting a patch formed by periodical alternation of low- and high-speed regions through the shock gives it a spanwise wrinkled aspect. When there is a lack of spanwise periodicity in the low/high velocity patches, the reflected

shockwave moves forward or backward, following the encounter with "relatively low, respectively high, speed flow regions".
These suppositions have been contradicted by Piponnau *et al.* [31], who compared conditional averaged velocity and Reynolds stresses profiles upstream of the oscillation region and found a difference of only 1% for a shock-imposed flow deflection angle of 8 °. For proving the existence of superstructures, "the order of magnitude of velocity difference between the superstructures with other structures should be on the order of $\pm 2u_\tau$" (see Ganapathisubramani *et al.* [11]), meaning around 20%. Moreover, the LES of Touber and Sandham [41] did not reveal any long enough boundary layer structures in the sense of the scaling proposed by Ganapathisubramani *et al.* [11] to induce an oscillation of the order $\mathcal{O}(10^2)$ Hz.

Andreopoulus and Muck [2] connected the shock motion in a compression corner flow case to bursting phenomena happening in the incoming boundary layer. The analysis of probability density functions of the periods and frequencies of the large structures embedded in the incoming turbulent boundary layer revealed a band of length scales which trigger the reflected shock oscillation and imprint it with ripples. Such events occur, however, at higher frequencies than the shock foot oscillation and, therefore, bursting cannot be directly responsible for it.

Another upstream effect on the interaction was thought to be the local thickening and thinning of the boundary layer. For a compression ramp flow, Ünalmis and Dolling found a correlation between the upstream Pitot pressure and the relative position of the shock: higher upstream pressure corresponds to an upstream displacement of the shock and vice versa. Although in the work of Beresh *et al.* [3] the mean velocity profiles for upstream and downstream shock excursions seem to not be correlated with boundary layer thickness evolution, hence not supporting the previous hypothesis of Ünalmis, the fluctuating streamwise velocity close to the wall seems to tell another story. There, "positive velocity fluctuations were correlated with downstream shock motions and vice versa. Furthermore, larger fluctuations corresponded to longer shock excursions".

One of the first attempts to intercorrelate the separation region dynamics with shock motion and incoming boundary layer was done experimentally by Erengil and Dolling [9]. From analysing the pressure signal before and in the interaction region, they distinguished essentially two mechanisms which would simultaneously govern the interaction: "one responsible for the large-scale sweeps, other for the high-frequency jitter that causes the shock foot to undergo a rapid series of changes in direction of motion [...]". The cause of the "large-scale sweeps" was not clarified in the study. A few years later, another referential experiment shed some light on the unsteadiness of shockwave-turbulent boundary

layer interaction: Dussauge *et al.* [8] characterised the reflected shock frequency motion by a Strouhal number range of 0.02−0.04. The Strouhal number was defined as $St = f_s L_{sep}/U_\infty$, where f_s is the characteristic frequency, L_{sep} is the average separation length expending from the average reflected shock position to the nominally shock impingement point and U_∞ is the freestream velocity prior to interaction. According to the authors, the lack of specificity in terms of characteristic Strouhal number might be due to the lack of generality of the chosen velocity, U_∞. Interestingly enough, the study revealed another important low frequency ($St \approx 0.5$) characterising the recirculating zone. There, the biggest energy aport is brought by these "higher" frequency structures, "low frequencies in the range involved by the shock motion contribute with about 25% of he total energy of the signal". This led to two conclusions: one was that the downstream events have little say in the upstream phenomena; second − there must be some sort of interference/correlation between the separated region dynamics and reflected shock translation. Indeed, one year later, in shock reflection experiments at $Ma = 2.3$ and different shock intensities, Dupont *et al.* [7] confirmed a non-dimensional frequency of $St = 0.03$ defining the shock movement. A slightly higher Strouhal number ($St \approx 0.04$) was calculated for the interaction zone. These frequencies were proven to "contribute up to 30% of the total energy of the pressure fluctuations" of the interaction zone. More than that, a phase shift of π was found between reflected shock and separation region dynamics. An exact relation between the two was not speculated.

A relatively new trend in trying to describe the shock dynamics is to relate it to both phenomena it enhances: separation bubble and shear layer encasing the bubble. Piponnau *et al.* [31] developed a formula for collapsing low frequencies found in different flow configurations and different Reynolds numbers (shock reflections and compression corners at different shock strengths): $St = St_L \times \{g(r,s)\Phi(M_c)\}^{-1}$. St_L is the Strouhal number based on the separation length and freestream velocity before the impingement, $g(r,s)$ has the formula 2.7 from Piponnau *et al.* [31] and is a function which characterises the intensity of separation region and $\Phi(M_c)$ quantifies the compressibility effects (its distribution over Mach number can also be found in the quoted paper). The conclusion of the study was that shock-boundary layer interaction has a rather universal behaviour, independent of flow parameters. More than that, it was found that the "downstream history of the flow" does not leave a mark on the unsteadiness phenomenon.

Exploring further the connection between the reverse flow bubble and inherent reflected shock motion, researchers (Pirozzoli *et al.* [33] and Touber and Sandham [41]) used the linear-stability analysis theory to find the governing modes of the interaction. After performing a very long LES, covering approximatively 90 low-frequency cycles, Touber found a 2-D globally unstable mode to be responsible for the bubble "breathing", with

corresponding time scales on the order of $10^2\delta_0/U_\infty$. These are considerably larger than the incoming turbulence. A Strouhal number $St = fL_{sep}/U_\infty \approx 0.03$ was also found to characterise the shock motion. Although Pirozzoli and his collaborators found the same global non-oscillatory mode in their LES, they additionally found "several oscillatory, weakly damped modes", which have frequencies comparable to the ones specific to the shock motion. Coincidence? As tempting as it would be to directly link these modes to the shock oscillation, they would need a driving mechanism to survive. Whether the answer to this question leads again to the analysis of the incoming boundary layer properties is not discussed in the paper, but it would seem hard to believe this is the point where a 36-years-of-research loop closes (in 1975 Plotkin postulated the effect of the upstream turbulent boundary on the interaction).

Before concluding the discussion about the origins of the low-frequency shock oscillation, there is another hypothesis which should be mentioned: after analysing the pressure covariance coefficients between different streamwise probes, Pirozzoli and Grasso [32] showed that due to the subsonic separated region and the shear layer forming on top of it, an acoustic feed-back loop forms, which seems to disturb the shock foot. Although they started their interaction DNS from a fully converged, naturally transitioned turbulent boundary layer (thus eliminating artificial frequencies produced by common inflow data generation methods), they were able, however, to simulate only $32\delta_0/U_\infty$ time units, while the bubble "breathing" motion has a specific time scale on the order of $10^2\delta_0/U_\infty$. Therefore, the acoustic resonance proposed by Pirozzoli still needs a reconfirmation.

However diverging the above mentioned studies were, their results seem to somehow evolve around specific quantities and values: it has been repeatedly found that an appropriate length scale for describing the SWTBLI is the average separation length, L_{sep} (see Garnier *et al.* [13], Priebe *et al.* [35], Pirozzoli *et al.* [33], and Pirozzoli and Grasso [32], Piponnau *et al.* [31], Touber and Sandham [41], Hadjadj *et al.* [15], Dupont *et al.* [7]). Consequently, a Strouhal number value of $St \approx 0.03$ emerges. The use of undisturbed freestream velocity, U_∞, might still be a reason for a few raised eyebrows, but because of the lack of other propositions, this too seems to give a satisfactory results.

Although the low-frequency problem is not yet completely clarified, there are other aspects of SWTBLI worth discussing.
First of all, one should be aware of the *marginal interactions*: cases where, due to freestream Mach number and the incident shock angle, β, the shock strength is not high enough to separate the boundary layer. At Pirozzoli *et al.* [33] we observe that the marginal flow deflection angle, θ, where low-frequencies begin to be noticed at the foot of the reflected shock is $\theta = 8°$. The same conclusion comes out from Piponnau *et al.* [31]

study, where a pressure spectra comparison was done for flow deflection angles between $\theta = 9°$, $\theta = 8°$ and $\theta = 5.5°$. The authors found a shift towards higher frequencies with decreasing θ, meaning the bubble dynamics, and therefore shock oscillation frequencies, were subject to change with decreasing the reverse flow size and shape.

Tridimensionality is another limiting effect of SWTBLI, which makes the comparison between experiments and numerical simulations subject to debate. In an experimental investigation of a 9.5° flow deflection angle SWTBLI configuration, Dussauge *et al.* [8] showed a PIV visualisation of the recirculation bubble. Its rhomboidal shape (Fig. 6 from Dussauge *et al.* [8]) was influenced by "tornado like" vortices. These 3-D structures were discovered on the tunnel walls. Puzzling enough, their characteristic frequency is around $200Hz$, value that corresponds to the average reflected shock oscillation frequency.
Further numerical investigations revealed the *influence of spanwise domain size* (see Touber and Sandham [41]) and *boundary conditions* (see Hadjadj *et al.* [15]). It is generally accepted that increasing the spanwise domain size is inversely proportional with the bubble length. For a $L_z = 5\delta_{int}$, where δ_{int} is the boundary layer thickness at interaction point in an undisturbed boundary layer simulation, Hadjadj ran simulations with spanwise periodic and slip boundary condition. The result was considerably different: corner vortices are forming on the bubble laterals, giving it a highly 3-D aspect, similar to the one observed by Dussauge *et al.* [8]. The flow confinement was found to increase the low frequency energy content. Therefore, the comparison between numerics and experiments should be considered with care. This conclusion is supported by Priebe *et al.* [35]. In his DNS, although reproducing the flow conditions from the experiment of Bookey *et al.* [4], was faced with important differences in terms of mean wall pressure distribution across the interaction.

Some studies linked *turbulence amplification* directly to the formation of a shear layer on top of the separated flow region. Plots of mass flux and Reynolds stresses at different locations in streamwsie direction of Loginov *et al.* [30] and Priebe *et al.* [35] prove this statement. It was found that streamline curvature acts as an enhancement for turbulence, as well as shocklet shedding after the reattachment point (see Loginov *et al.* [30]).

Due to its possible contribution to fuel/air mixing, in the present study we investigated the turbulence amplification mechanism. We do not consider multiple species. The aim of the study is to look at SWTBLI from the turbulence production perspective and means to amplify it.

2.1.3 Shockwave-Entropy Spot Interaction

Earlier on, we have seen the complexity evolving around the flow in scramjet propulsion system: shockwaves dominate the entire engine flow path, inlet to nozzle. Any other additional phenomena present in the flow (e.g. fuel injection, mixing, combustion, turbulence, etc) has to endure interaction with shocks. In most of the cases this interplay results in mutual effects. If we consider fuel/air mixing enhancement, we are interested in the situations which have as one of the results turbulence amplification.
The scramjet configuration adopted within GRK 1095 (see Fig. 1.3) has a strut injector located in the middle of the first half of the combustion chamber, and two ramp injectors on opposite walls in the second diverging part of the combustor. As a consequence, it is rather easy to imagine a scenario where fuel is injected through the upstream wedge and is mixed and burned as is convected with U_∞ downstream; the pressure increase due to combustion triggers the formation of a shock train which dominates the flow; in these conditions we might be faced with "patches" of hot or cold fluid convecting through incident-reflected shock systems. A hot patch is a region with higher temperature resulted from burned fuel, while a cold patch is a region rich in unburned fuel. The denotation of "hot" or "cold" is made based on the relative temperature of the "patches" with respect to the surrounding fluid temperature. For simplicity and obeying previous nominations existing in literature, we will further refer to the hotter or colder regions as to *entropy spots* (ES).

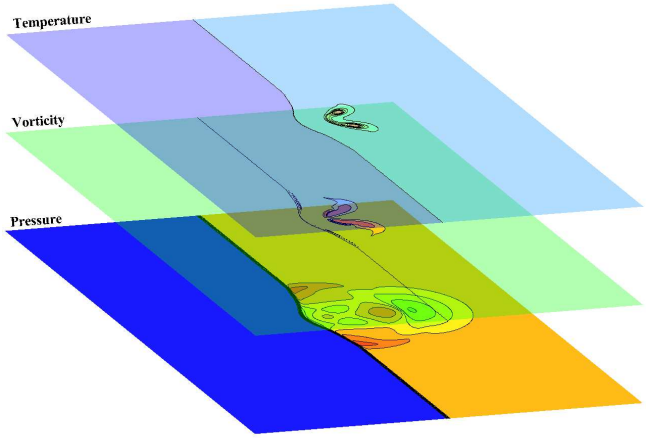

Figure 2.2: Shockwave-entropy spot interaction

The interaction of an ES with a shockwave has been investigated over the past decades (see Hussaini and Erlebacher [25] or Fabre *et al.* [10]). The phenomenon results in: deformation towards an ellipsoid of the formally round ES; deformation of the shock front exposed to the ES convection due to low pressure region existent in the ES core; formation and propagation of an acoustic wave in the region downstream of the shock; formation of two pairs of counterrotating vortices due to post-shock fluid baroclinicity (see Fig. 2.2). It is this vorticity production that posses an interest in the supersonic combustion frames described earlier.
In 1950s, the Linear Interaction Approximation (LIA) Theory was developed by Ribner [36] in order to analyze the shock-turbulence interaction and be able to quantify experimental results. The assumptions involved are not restrictive (see Garnier *et al.* [12]), making the theory widely applicable. Following Kovasznay's decomposition of the fluctuating flow field in entropy, vorticity and acoustic modes, authors have successfully used LIA for analysing the interaction of vorticity-dominated turbulence, mixed-mode turbulence (acoustic/vortical or entropic/vortical) or entropy-dominated turbulence with a shockwave. A comprehensive inventory is to be found at Garnier *et al.* [12].
Previous investigations on shock-ES interaction were limited either to normal shocks (Hussaini and Erlebacher [25] or Fabre *et al.* [10]), relatively weak ES amplitudes (25% of the surrounding fluid temperature at Hussaini and Erlebacher [25]) and/or only positive amplitudes, respectively only hot ES. Although Fabre *et al.* [10] found an "excellent" qualitative and quantitative agreement with LIA for the convection of an ES with a GAUSSian distribution through a shock, inducing the conclusion that the interaction is an essentially linear phenomenon, the results of Hussaini are a bit surprising: from his 2-D simulation he concluded that "cold spots generate stronger maximum vorticity than hot sports". This, together with turbulent kinetic energy, Reynolds stresses, mass flux amplifications are matters tackled in the present study.

We first addressed a 2-D flow scenario (ES-normal shock interaction) in the Appendix to set a prerequisite for our simulations, where a spheroidal ES is let to convect through a normal schockwave.

— CHAPTER THREE —

NUMERICAL METHOD

3.1 Notes on Implicit LES Modeling

We have previously presented the frames of this work, the motivation behind it and what we hope to find. For scientific credibility, it makes sense we now introduce the computational method employed in this study. Before starting on this matter, we wish to stress that this chapter will merely be like a candle in the darkness of Computational Fluid Dynamics (CFD), meant to give a sense of direction for the reader, rather than a blueprint of the numerics used here. The reason for this is simple: the shear numerical modelling and testing we relied on in this study is somebody else's story to tell. And this will, of course, be correspondingly referenced.

Given their size, flow simulations of current industrial applications are addressed by means of Reynolds Averaged Navier-Stokes (RANS) equations. As the name says it, the outcome of these simulations is, in most of the cases, temporally averaged, the turbulent scales are all contained in one model, represented by one or more equations. This may very well be an appropriate choice for conducting a study, if what we are dealing with are stationary or periodic well-established flows. With RANS, as my professor used to say, "we can fool around, as usual".

If we care for exploring a certain phenomenon in more detail, gaining knowledge into flow physics, as well as into turbulence, we might want to look other ways for getting reliable results. Direct Numerical Simulations (DNS) rapidly fall out from the competition, given the exhaustive computational resources needed. The compromise between the RANS and DNS are Large Eddy Simulations (LES). This method appears to be suited for a shockwave-turbulent boundary layer interaction flow phenomenon, where the flow physics is known (shock reflection and boundary layer separation), and yet there are still some features, such as oscillation of the reflected shockwave, which require a flow representation able to capture unsteady characteristics of the field.

Assuming a finite volume discretisation of the computational domain and that the flow is fully turbulent, in LES the flow is computed down to the size of the finest grid cell, this commonly being considered as the filter width. The rest of the turbulent scales, down to Kolmogorov length scale, are encompassed in the simulation by modelling their effect on the larger scales, through the so-called *subgrid-stress tensor* (SGS tensor). This modelling can be done *explicitly* or *implicitly*. For better understanding, let us

briefly consider a general conservation law:

$$\frac{\partial}{\partial t}u + \frac{\partial}{\partial x}F(u) = 0. \tag{3.1}$$

After filtering and discretising, this equation will come to the form

$$\frac{\partial}{\partial t}\overline{u}_N + \frac{\partial}{\partial x}\overline{F(\overline{u}_N)} = \tilde{\mathcal{G}}_{SGS} + \mathcal{G}_{num}, \tag{3.2}$$

where the over-bar denotes the filtering operation and the index "N" represents the numerical discretisation process. The right hand-side term from Eq. (3.2) shows the interference between the subgrid-scale tensor, $\tilde{\mathcal{G}}_{SGS}$, and the numerical truncation error, $\mathcal{G}_{num}$. The intuitive approach for numerically solving the above mentioned transport equation is to model the subgrid-scale tensor as physically plausible as possible and minimise the truncation error. These are the so-called *explicit* LES turbulence models. The most popular one is the Smagorinsky-Lily eddy viscosity model. Given the fact that the SGS model operates on the smallest scales captured by the numerical grid, the solution evidently falls under the incidence of the discretisation scheme. Therefore it can come to cases when the resulting truncation error outweighs the SGS model (see Johnsen *et al.* [26] and Ghosal [14]). This can lead to incorrect solutions, lack of grid convergence, numerical stability issues for higher order schemes, etc.
There is, however, another way to close in on this matter; that is to exploit this mutual interference between the numerical truncation error and the SGS model (used in the *implicit* LES). In other words, the truncation error resulting from the discretization scheme is fully merged with the turbulence model.
In the current study, we used the Adaptive Local Deconvolution Model (ALDM) as the implicit LES model for representing turbulent scales. As we mentioned in the beginning of this chapter, the numerical background and reasoning behind ALDM were or will be presented elsewhere (Hickel [17], Hickel [16], Hickel and Larsson [22]). In these pages we will only try to catch it all in a nutshell.
The realization of an implicit turbulence model implies three steps:
1. **Design** a discretisation scheme with a controllable truncation error;
2. **Analyse** the discretisation scheme;
3. **Optimise** the truncation error such that it is loyally represents subgrid-scale stresses.

According to Hickel [17], after employing all these steps, the result was "a nonlinear fine volume scheme based on a solution-adaptive deconvolution operator and a numerical

flux function that [already] incorporates the essential reasoning of LES, filtering and deconvolution. Explicit deconvolution-type SGS models have been so far limited to linear deconvolution. ALDM extends the concept of approximate deconvolution to the solution-adaptive nonlinear case. [...] Free parameters inherent to the discretisation allow to control the truncation error and have been calibrated in such a way that the truncation error acts like a physically motivated SGS model" (Hickel and Larsson [22]). The resulting turbulence model was successfully tested for various incompressible flows scenarios: 3-D isotropic turbulence (Hickel *et al.* [20]), transitional and turbulent wall-bounded flows (Hickel and Adams [18]), boundary layer separation (Hickel and Adams [19]), wake vortex flows (Klar *et al.* [28]) and passive-scalar mixing (Hickel *et al.* [21]).
The extension to compressible turbulent flows was not trivial. The reasons for this are two-fold: *first of all*, in the incompressible case, only the prediction of the energy decay-rate is necessary for accurately representing the flow, while in the compressible case, we also need de decay-rates of density, temperature, pressure and dilatation fluctuations, because, in the sense of Kovasznay, turbulence is modelled correctly when all of acoustic, vortical and entropy modes are properly represented; the *second* challenge in correctly modelling turbulence with LES is that the subgrid-scales that don't make the cut and are not computed in the simulation (but whose effects are just modelled), can contain various structures which require divergent numerical treatments, such as small-scale turbulence and shockwaves. The adaptation to compressibility for ALDM was accomplished already and its consequent publication is on-going work (Hickel [16]). A start-up point for this subject can be found at Hickel and Larsson [22].

3.2 Application to the Navier-Stokes Equations

In the present section we wish to highlight the key-points when applying ALDM to the Navier-Stokes equations (NSE).
We consider the 3-D NSE written in conservative form,

$$\frac{\partial}{\partial t}U + \nabla \cdot \mathbf{C}(\mathbf{U}) + \nabla \cdot \mathbf{P}(\mathbf{U}) + \nabla \cdot \mathbf{D}(\mathbf{U}) = \mathbf{0}. \tag{3.3}$$

U is the solution vector, $U = [\rho, \rho u_1, \rho u_2, \rho u_3, \rho E]$, which contains the conserved variables: density ρ, momentum ρu_i and total energy E. $\mathbf{C}$ is convective term given by

$$\mathbf{C_i} = \begin{bmatrix} u_i\rho \\ u_i\rho u_1 \\ u_i\rho u_2 \\ u_i\rho u_3 \\ u_i\rho E \end{bmatrix}. \tag{3.4}$$

P and **D** give the stresses due to pressure and viscosity and have the form

$$\mathbf{P_i} = \begin{bmatrix} 0 \\ \delta_{i1}p \\ \delta_{i1}p \\ \delta_{i3}p \\ u_k\delta_{ik}p \end{bmatrix}, \mathbf{D_i} = - \begin{bmatrix} 0 \\ \tau i1 \\ \tau i2 \\ \tau_{i3} \\ u_k\tau_{ik} + q_i \end{bmatrix}. \tag{3.5}$$

u_i represents the velocity vector, τ_{ij} is the viscous stress tensor for a Newtonian fluid and

$$\tau_{ij} = \mu(T)\left(\partial_j u_i + \partial_i u_j - \frac{2}{3}\delta_{ij}\partial_k u_k\right). \tag{3.6}$$

q_i from **D** in Eq. (3.5) represents the heat flux and is temperature-dependent with the formula

$$q_i = k(T)\partial_i T. \tag{3.7}$$

Constitutive relations close the NSE system.
The viscosity is temperature-dependent by the powerlaw

$$\mu(T) = \frac{T^{0.75}}{Re}. \tag{3.8}$$

The thermal conductivity, k is given by

$$k(T) = \frac{\mu(T)}{(\gamma - 1)PrMa^2}. \tag{3.9}$$

The equation of state and the definition of internal energy relate pressure and temperature through

$$T = \frac{p}{\rho}\gamma Ma^2 \tag{3.10}$$

and

$$\rho e = \rho\left(E - \frac{1}{2}u^2\right) = \frac{1}{\gamma - 1}p. \tag{3.11}$$

The fluid is assumed to be ideal gas with the parameters $Pr = 0.72$, specific heats' ratio $\gamma = c_p/c_v = 1.4$ and with the non-dimensional parameters the Reynolds (Re) and Mach (Ma) numbers.

In Section 3.1 we have elaborated on the novelty of ALDM. In the finite volume framework, using this turbulence model involves three numerical steps: "reconstruction of the unfiltered solution at cell faces, a numerical flux function that works on the reconstructed solution and a numerical integration scheme to recompute the face-averaged flux" (Hickel [16]). The reconstruction and numerical flux function computation steps make use of three sets of free parameters. It is because of these parameters that the truncation error of the discretisation scheme can be manipulated such that it acts as a physical subgrid-scale turbulence model. The ideal set of parameters results from employing an evolutionary algorithm, which aims at minimizing the difference between the effective spectral numerical viscosity of ALDM and the eddy viscosity from the Eddy-Damped Quasi-Markovian (EDQNM) theory for isotropic turbulence. Although not treated in the finest detail, currently, the most elaborate work on the compressible ALDM can be found in the paper of Hickel and Larsson [22]. Another, more comprehensive paper is on the way (Hickel [16]).
In the case of the NSE, ALDM was used only for the computation of the inertial term, ($\mathbf{C_i}$), given by Eq. (3.4). The viscous part was computed using a second order central difference scheme. The time integration was achieved with a third order Runge-Kutta method.
The challenge of the current computational case, shockwave-turbulent boundary layer interaction, resides, as mentioned earlier in this work, in accurately representing both turbulence and shockwaves, since the phenomena require opposing numerical treatments: shocks need artificial numerical dissipation in order to be sharply represented, while turbulence does not. Based on this knowledge, based on the idea of Ducros *et al.* [6], we

used a so-called "shock-sensor", in order to detect discontinuities and treat them differently, respectively by adding an extra-dissipation term in computing the numerical flux function (for more details see Hickel [16]).

The boundary conditions used in the simulations we performed will be explained as we go along.
An always useful clarification is the direction of the coordinate system we used: positive X direction is the flow direction, positive Y is the wall-normal coordinate and positive spanwise direction follows from them.